Precision Measurement of Trident Production in Strong Electromagnetic Fields

Christian F. Nielsen,[1] Robert Holtzapple,[2] Mads M. Lund,[1] Jeppe H. Surrow,[1] Allan H. Sørensen,[1] Marc B. Sørensen,[1] and Ulrik I. Uggerhøj[1]

(CERN NA63)

[1]*Department of Physics and Astronomy, Aarhus University, 8000 Aarhus, Denmark*
[2]*Department of Physics, California Polytechnic State University, San Luis Obispo, California 93407, USA*

(Received 28 October 2022; accepted 20 January 2023; published 14 February 2023)

We demonstrate experimentally that the trident process $e^- \to e^-e^+e^-$ in a strong external field, with a spatial extension comparable to the effective radiation length, is well understood theoretically. The experiment, conducted at CERN, probes values for the strong field parameter χ up to 2.4. Experimental data and theoretical expectations using the local constant field approximation show remarkable agreement over almost 3 orders of magnitude in yield.

DOI: 10.1103/PhysRevLett.130.071601

Introduction.—An electron interacting with an electromagnetic field may generate an electron-positron pair, resulting in three emerging particles, hence the name trident. As shown in one of the first applications of relativistic quantum theory in 1929 by Klein [1], an undamped electron current is present beyond the classical turning point when an electron is incident on a high and steep potential barrier. Sauter [2,3], inspired by a supposition by Bohr, soon after showed that the corresponding field is required to provide an increment in potential energy of order the rest energy of the electron, mc^2, over its Compton wavelength, $\hbar/mc$. While the existence of the positron was unknown in 1929, the modern interpretation of the "Klein paradox" thus implies that the necessary field strength for the direct trident process $e^- \to e^-e^+e^-$ to happen in a strong external field is of order

$$\mathcal{E}_0 = m^2c^3/e\hbar \simeq 1.32 \times 10^{16}\ \mathrm{V/cm}, \tag{1}$$

which is known as the critical or Schwinger field. The Klein paradox has in recent years attracted some attention for analogous systems in graphene [4–8].

Although the present experiment does not investigate the Klein paradox *per se*, it demonstrates experimentally that the trident process $e^- \to e^-e^+e^-$ becomes significant when an external field of strength approaching $\mathcal{E}_0$ is present. In our experiment we obtain this field by rotating a crystal, relative to the beam direction, from a "random" orientation, where the field experienced by a penetrating particle is the sum of essentially randomly placed screened Coulomb fields, to an axial orientation, where the atoms along the axis act coherently in deflecting the particle. This effectively creates a continuous field which is macroscopic along the main direction of motion and of critical magnitude in the particle rest frame.

Regardless of the orientation of the crystal, there are two contributions to the trident process, the direct and a "two-step" or "cascade" contribution, where the incoming electron first emits a real photon which then converts to an electron-positron pair. In our case, the direct trident production, the emission of real photons, and conversion of photons into pairs, all proceed in essentially constant fields.

The trident process for electrons penetrating amorphous material where they interact with screened target nuclei, has been investigated in detail since the 1930s, see, e.g., [9–20]. As a result, the amorphous yield of trident events is considered well known and the contributions to the total trident yield for the direct and two-step processes are similar for material thicknesses of a few percent of the radiation length X_0 [17,20]. For the aligned crystal in our experiment, the effective radiation length is much shorter than X_0 due to strong-field effects. It is comparable to the crystal thickness and, in consequence, the two-step process dominates the trident production.

For extended electromagnetic fields, the trident process depends on the strong-field parameter χ defined through [21–23]

$$\chi^2 = (F_{\mu\nu}p^\nu)^2/m^2c^2\mathcal{E}_0^2, \tag{2}$$

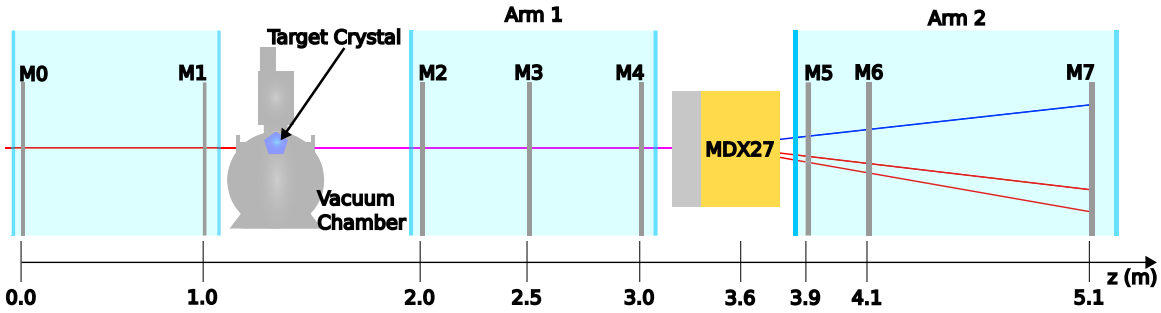

FIG. 1. Experimental setup. A schematic representation of the experimental setup in the H4 beamline in the SPS North Area at CERN. The symbols "Mi," with $i = 0, \ldots, 7$, denote "Mimosa-26" position sensitive detectors.

where $F_{\mu\nu}$ is the electromagnetic field strength tensor and p^{ν} is the four-momentum. For values of χ smaller than unity, pair production by photons is exponentially suppressed [21,22], therefore the trident process is also suppressed. Consequently, the scale of the electric fields, $\mathcal{E}$, required for the trident process to occur is of the order $\mathcal{E}_0$ for modest momenta. Such fields are not yet possible to produce in the laboratory. However, a relativistic particle, with a relatively large Lorentz factor, e.g., $\gamma \simeq 10^5$–10^6, will experience an electric field in its own rest frame that, with a suitable field configuration, may be Lorentz boosted and can reach $\chi > 1$, which enables the trident process. The trident process in plane wave background fields has been, and is being investigated in great detail, both experimentally (SLAC-E144 experiment [24]) and theoretically (see, e.g., the comprehensive review [25] and references therein). Most theoretical investigations are driven by several upcoming and ongoing experiments colliding GeV electron beams with tightly focused laser pulses to probe the trident process [26,27].

Aligned crystals have been a known source of strong electric fields for decades, see, e.g., [22,28] for details on strong field effects in crystals. Depending on the element and orientation of the crystal, fields of the order 10^9–10^{11} V/cm are readily available in the laboratory frame. Because of the coherent action of the screened nuclei along crystallographic directions, this field is of truly macroscopic extent for Ge and Si crystals, where single crystals can be grown in principle to meters in length. For a charged particle moving in a field that is purely electric in the laboratory, and essentially transverse to the direction of motion as in the case of an aligned crystal, the strong field parameter reduces to $\chi \simeq \gamma\mathcal{E}/\mathcal{E}_0$. At CERN, electrons and positrons with up to $\gamma \simeq 10^6$ are available making it possible to achieve values of $\chi > 1$ in the rest frame of the electron in an aligned crystal.

In 2007 an attempt to measure the production of electron-positron pairs through the trident process $e^- \to e^-e^+e^-$ in strong electromagnetic fields was made with participation from one of the present authors (U. I. U.) [29], that resulted in significant discrepancies with theory. In this Letter we report on a recent precision measurement of the trident process, impinging 200 GeV electrons on the same 400 μm germanium crystal target as in 2007, oriented along the ⟨110⟩ axis, showing an extraordinary agreement between theory and experiment. Thus, the discrepancies observed in the 2007 experiment are yet to be explained. It is our conjecture that the 2007 experimental values are incorrect possibly due to improper alignment of the crystal.

Experiment.—The experiment was performed by the NA63 Collaboration at the H4 beamline of the CERN SPS that provided a 200 GeV electron beam having a $\sigma_x \simeq \sigma_y \simeq 105$ μrad divergence impinging on the 400 μm thick ⟨110⟩ oriented germanium single crystal. Figure 1 is a schematic of the setup where M0–M7 are MIMOSA-26 position sensitive CMOS-based pixel detectors [30]. The detectors have a resolution of a few μm and an active area of 1.1×2.1 cm^2 containing 576×1152 pixels. The crystal target is mounted on a goniometer that allows us to set the crystal orientation with μrad precision. The MDX27 magnet provides an integrated magnetic field of 0.072 Tm and, together with the detectors in arm 1 and arm 2, forms a magnetic spectrometer allowing us to measure the energy of each charged particle from the deflection angle in the magnet. The crystal is situated inside a vacuum chamber at ≃300 K. To reduce scattering and background, all mimosas are placed in closed compartments that are continuously flushed with helium. The total material contributing to the background before the MDX27 magnet, in units of the radiation length, amounts to ≃1.1%.

The incoming electron rate was set to ensure that only a single primary electron was present in the setup per event. We therefore have essentially complete information about the particle and its secondaries.

Three measurement series were performed; a background measurement with no target, a "random" measurement where the crystal was rotated far away from any major crystallographic orientation thus acting as an amorphous target, and a measurement with the aligned crystal. In the latter, the crystal was aligned with the beam centroid along the ⟨110⟩ axis through a careful procedure where enhancement of radiation upon the passage of crystalline planes creates a stereogram from which the location of the axis can be found with a precision of about 20 μrad.

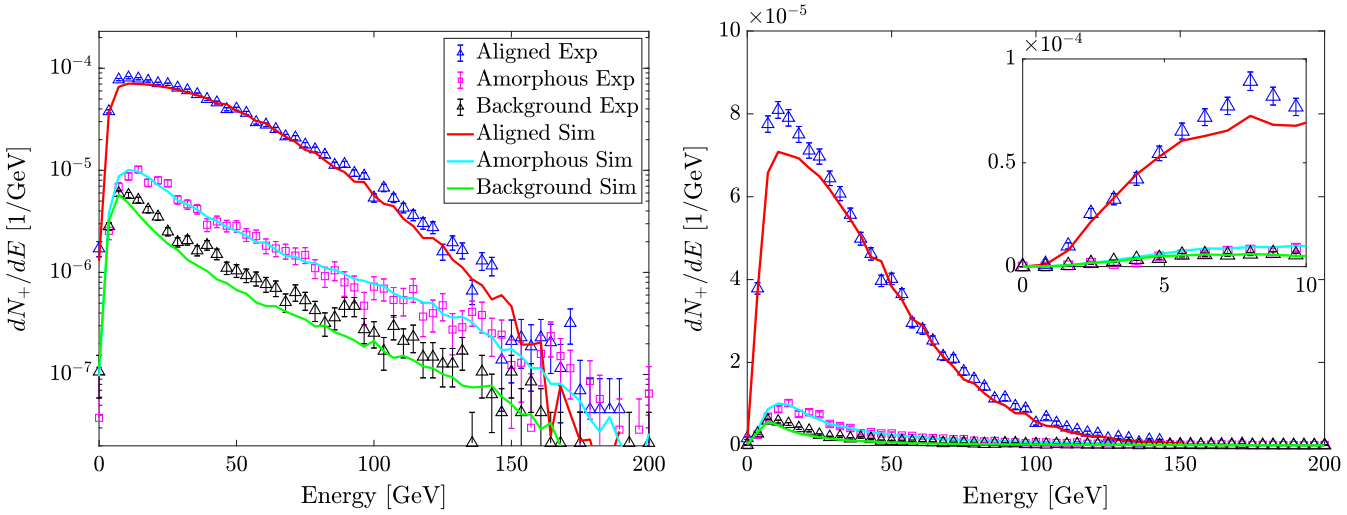

FIG. 2. Positron spectrum of reconstructed trident events. Solid lines are simulations while squares and triangles are experimental data points. Blue and red show the trident spectrum in aligned orientation, magenta and cyan show the amorphous yield while black and green is the background. The right figure is the same as the left but with a linear vertical axis. The inset shows a zoom of the low energy part, which largely overlaps with the energy range measured in 2007 [29].

Data analysis and theoretical comparison.—The data analysis routine begins by finding complete single particle tracks after the target by matching tracks, found in arm 1 and arm 2, in the center of the magnet. A track in arm 1 is only accepted if it simultaneously overlaps with a hit in M0 and M1. The energy resolution of the magnetic spectrometer for a single particle track was measured to be $\sigma_E/E \simeq 6.7\%$ at 200 GeV (including $dp/p \simeq 1\%$ from the beamline) and it remains relatively uniform down to particle energies of a few GeV.

To find possible trident events, all complete single particle tracks are matched through strict matching criteria to form a triplet event with a single positively charged and two negatively charged particles. A trident event is only confirmed if all three particles can be identified and matched to originate from a single primary particle and, at the same time, have a small separation inside the MDX magnet. The setup provides complete information on the angle of each particle, together with the differential energy distribution [31].

Figure 2 shows the experimentally measured positron spectrum of all three measurement series together with theoretical predictions. The theoretical curves labeled "Sim" result from a full scale Monte Carlo simulation of the experimental setup, starting with a beam of electrons identical to what was provided by the SPS. A two-sample Kolmogorov-Smirnoff test was performed [32] with the experimental and simulated data. It resulted in a p value of $p = 0.99$, which strongly suggests that the experimental and simulated aligned curves are drawn from the same distribution. The simulation propagates primary electrons individually through each element of the setup, where they are subject to multiple Coulomb scattering and emission of photons, that can later pair produce, and direct trident production. When a particle penetrates a detector, its position is saved in a data file identical to the experimental data file containing (x, y, z) positions from each detector from particle hits. The simulated data files are then analyzed with the experimental analysis routine. As in the experiment, we simulate all three measurement conditions and the background is subtracted from the amorphous and aligned curves after the analysis. To account for detector efficiencies, we fit a linear energy dependent efficiency, $f(E) = aE + b$, to the ratio between the experimental and simulated curves for the amorphous case after background subtraction. All simulated curves shown in Fig. 2 are then the result of the experimental analysis routine multiplied by the linear energy efficiency factor with the fitting parameters $a = -0.0009 \pm 0.001$ GeV^{-1} and $b = 0.85 \pm 0.08$. The value for b, found by this procedure, agrees well with expectations based on the efficiency of the Mimosa detectors that depend on set threshold values, and the value of a is small.

When particles penetrate amorphous material, the probability of the two-step trident process is modeled by Bethe-Heitler photon emission followed by Bethe-Heitler pair production as described in, e.g., [33]. The scattering centers are completely decoupled and nonlinear effects, e.g., photons emitted in the background that pair produce in the crystal or vice versa, are then taken into account by the simulation of the experiment. Therefore, it is important that all elements are included correctly in the setup and that the background simulation matches the measurement. The direct trident process is modeled using the theory described in [17,20]. Amorphous material in the background and the crystal oriented in "random" are modeled identically, the

processes depend on the nuclear charge Ze and the radiation length X_0. Figure 2 shows that the theoretical curves and experimental data are in good agreement for the amorphous case, as in the 2007 experiment [29]. Using the detector-efficiency correction on the background, we also see good agreement, which strongly indicates that the background contribution is well understood.

When a particle hits the aligned crystal, a separate simulation code is employed which is described in detail in [34,35]. The simulation solves the equation of motion for each time step based on the Lorentz force in the electric fields modeled by the Doyle-Turner continuum string potentials [36,37]. For every time step the local value of χ is evaluated and the probability of photon emission is calculated under the assumption that the external electromagnetic field is locally constant, the local constant field approximation (LCFA), see, e.g., [21,22] for derivations. Incoherent scattering on target atoms, as well as photon emission due to such scattering, is also included [38]. The photon is then propagated forward through the crystal where the probability of pair production, again using the LCFA and including an incoherent contribution [38], is evaluated and the produced pair is propagated through the experimental setup (details on the implementation of these processes can be found in [35]).

The applicability of the LCFA requires that the external electromagnetic field is constant over the formation length [28,39]. This is satisfied in crystals when the angular excursions of the projectile over a formation length are wider than the light cone $1/\gamma = 2.6$ μrad. In the channeling regime, the angular excursions of a charged particle are on the order of the critical Lindhard angle [37,40], which in our case is 57 μrad. For entry angles larger than the critical Lindhard angle, but smaller than the Baier angle $U_0/mc^2 = 0.4$ mrad, the angular deflections remain larger than $1/\gamma$ [38]. Here $U_0 = 215$ eV is the continuum string potential depth, in this case for a single $\langle 110 \rangle$ row of Ge atoms. As a result, for a beam with a divergence of $\simeq$105 μrad aimed at the aligned crystal, the LCFA is appropriate for nearly all particles. See, e.g., [39,41] for studies on the applicability of the LCFA in crystals and short focused laser pulses. As a measure of the applicability of the constant-field approximation under channeling conditions, the authors of [22] introduced the parameter $\rho_c = \xi^2 = 2U_0\gamma/mc^2$ (where ξ is known as the classical nonlinearity parameter [25,42] in the strong-field laser community), which under channeling conditions has a value of $\simeq$330 for 200 GeV electrons. The large value of ρ_c verifies that treating the local field as constant is a good approximation.

For the aligned crystal, the direct trident process is modeled through the Weizsäcker-Williams method of virtual quanta [22,43], together with the LCFA and the incoherent contribution for the pair production vertex. For constant electric fields, the Weizsäcker-Williams method has been investigated and deviates around 10% from methods evaluating the actual direct two-vertex Feynman diagrams [44,45]. This difference has marginal influence in our case due to the dominance of the two-step process.

Figure 2 shows that the theoretical prediction for the aligned case agrees remarkably well with the experimental data points throughout the entire spectrum which spans several orders of magnitude.

The relative importance of the direct process and the two-step process can be estimated by comparing the virtual Weizsäcker-Williams photon intensity (radiated energy per photon-energy interval) with the real photon intensity. The virtual photon intensity is given by the fine-structure constant up to a logarithmic factor. The real photons have a fairly flat intensity spectrum given by L/X, where L is the target thickness and X the effective radiation length defined as $X = E/(dE/dx)$ where dE/dx is the energy-loss rate per unit length due to radiation. Therefore, the two processes are comparable in strength for a target thickness of order a percent of the effective radiation length (see also [44,46,47]). This is the case for the amorphous setting in our experiment ("random" setting), where $X = X_0 = 2.30$ cm and $L/X_0 = 1.7\%$. Accordingly, the simulations show that ~50% of all tridents come from the direct process in the amorphous setting. For the aligned case, the effective radiation length X is much shorter than X_0 due to the strong-field effects. The stronger radiation causes the direct process to only contribute a few percent to the total pair rate.

In the two-step process, the theoretical model applied averages over the photon polarization. The polarization has been predicted to have significant effects in strong constant fields [48,49]. For axially aligned crystals, the experimentally measured photon spectrum is polarization averaged due to each projectile having a unique trajectory through the crystal. If a real photon is emitted with a specific polarization, this photon will also follow a unique trajectory due to the uniqueness of the emitting particle. This means the pair production process also becomes polarization averaged, and modeling the real photon as unpolarized, is a good approximation.

Conclusion.—By impinging 200 GeV electrons on a $\langle 110 \rangle$ oriented 400 μm thick germanium crystal, we investigated the trident process in strong electric fields. Our experimental results are in remarkably good agreement with theory based on LCFA, the locally constant field approximation.

The inset in Fig. 2 shows the low-energy tail (which is subject to a major nonlinear drop in detection efficiency) corresponding to the energy range studied in the 2007 experiment [29]. Here too, there is good agreement between theory and experiment. Accordingly, the discrepancy in 2007 most likely was due to improper alignment of the target crystal.

In our case the experimental spectrum is dominated by the two-step process. To quantify the direct process using an aligned crystal, the crystal will have to be much thinner

than what was used here. An ultrathin crystal greatly reduces the production rate, making it a challenging measurement, even if the crystal is cooled.

We would like to thank Erik Larsen and Frank Daugaard for their enthusiasm and superb technical assistance during the experimental run. The numerical results presented in this work were partly obtained at the Centre for Scientific Computing Aarhus (CSCAA) and with support from Nvidia's GPU grant program. This work was partially supported by the U.S. National Science Foundation (Grants No. PHY-1535696 and No. PHY-2012549) and from the Danish National Instrument Center for CERN Experiments (NICE).

[1] O. Klein, Z. Phys. **53**, 157 (1929).
[2] F. Sauter, Z. Phys. **69**, 742 (1931).
[3] F. Sauter, Z. Phys. **73**, 547 (1931).
[4] M. Katsnelson, K. Novoselov, and A. Geim, Nat. Phys. **2**, 620 (2006).
[5] A. Calogeracos, Nat. Phys. **2**, 579 (2006).
[6] M. Buchanan, Nat. Phys. **2**, 721 (2006).
[7] P. Bøggild, J. M. Caridad, C. Stampfer, G. Calogero, N. R. Papior, and M. Brandbyge, Nat. Commun. **8**, 15783 (2017).
[8] V. H. Nguyen and J.-C. Charlier, Phys. Rev. B **97**, 235113 (2018).
[9] H. R. Crane and J. Halpern, Phys. Rev. **55**, 838 (1939).
[10] C. F. Powell, Il Nuovo Cimento (1943–1954) **6**, 379 (1949).
[11] G. P. S. Occhialini, Il Nuovo Cimento (1943–1954) **6**, 413 (1949).
[12] J. Hooper, D. King, and A. Morrish, Lond. Edinb. Dubl. Phil. Mag. J. Sci. **42**, 304 (1951).
[13] W. H. Barkas, R. W. Deutsch, F. C. Gilbert, and C. E. Violet, Phys. Rev. **86**, 59 (1952).
[14] J. Hooper, D. King, and A. Morrish, Lond. Edinb. Dubl. Phil. Mag. J. Sci. **43**, 853 (1952).
[15] M. M. Block, D. T. King, and W. W. Wada, Phys. Rev. **96**, 1627 (1954).
[16] W. Heitler, *The Quantum Theory of Radiation*, 3rd ed. (Oxford University Press, London, 1954).
[17] S. R. Kel'ner, J. Nucl. Phys. (U.S.S.R.) **5**, 1092 (1967) [S. R. Kel'ner, Sov. J. Nucl. Phys. **5**, 778 (1967)].
[18] B. Grossetête, R. Tchapoutian, D. J. Drickey, and D. Yount, Phys. Rev. **168**, 1475 (1968).
[19] J. Böhm, A. Mátlová, J. Trková, and Z. Trka, Nucl. Phys. **B57**, 355 (1973).
[20] V. N. Baier and V. M. Katkov, JETP Lett. **88**, 80 (2008).
[21] V. I. Ritus, J. Sov. Laser Res. **6**, 497 (1985).
[22] V. N. Baier, V. M. Katkov, and V. M. Strakhovenko, *Electromagnetic Processes at High Energies in Oriented Single Crystals* (World Scientific, Singapore, 1998), p. 554.
[23] V. B. Berestetskii, E. M. Lifshitz, and L. P. Pitaevskii, *Quantum Electrodynamics* (Pergamon, New York, 1989).
[24] C. Bula, K. T. McDonald, E. J. Prebys, C. Bamber, S. Boege, T. Kotseroglou, A. C. Melissinos, D. D. Meyerhofer, W. Ragg, D. L. Burke, R. C. Field, G. Horton-Smith, A. C. Odian, J. E. Spencer, D. Walz, S. C. Berridge, W. M. Bugg, K. Shmakov, and A. W. Weidemann, Phys. Rev. Lett. **76**, 3116 (1996).
[25] A. Fedotov, A. Ilderton, F. Karbstein, B. King, D. Seipt, H. Taya, and G. Torgrimsson, arXiv:2203.00019.
[26] H. Abramowicz *et al.*, Eur. Phys. J. Spec. Top. **230**, 2445 (2021).
[27] E-320 Collaboration, Probing Strong-Field QED at FACET-II (unpublished experimental proposal, 2018).
[28] U. I. Uggerhøj, Rev. Mod. Phys. **77**, 1131 (2005).
[29] J. Esberg, K. Kirsebom, H. Knudsen, H. D. Thomsen, E. Uggerhøj, U. I. Uggerhøj, P. Sona, A. Mangiarotti, T. J. Ketel, A. Dizdar, M. M. Dalton, S. Ballestrero, and S. H. Connell (CERN NA63 Collaboration), Phys. Rev. D **82**, 072002 (2010).
[30] J. Baudot, G. Bertolone, A. Brogna, G. Claus, C. Colledani, Y. Degerli, R. De Masi, A. Dorokhov, G. Dozière, W. Dulinski, M. Gelin, M. Goffe, A. Himmi, F. Guilloux, C. Hu-Guo, K. Jaaskelainen, M. Koziel, F. Morel, F. Orsini, M. Specht, I. Valin, G. Voutsinas, and M. Winter, in *2009 IEEE Nuclear Science Symposium Conference Record (NSS/MIC)* (IEEE, Manhattan, New York, 2009), pp. 1169–1173.
[31] A comprehensive paper is being prepared which details the data analysis and simulations and includes e.g. analysis of differential spectra and angular information.
[32] F. J. Massey, J. Am. Stat. Assoc. **46**, 68 (1951).
[33] R. L. Workman *et al.* (Particle Data Group), Prog. Theor. Exp. Phys. **2022**, 083C01 (2022).
[34] C. F. Nielsen, Comput. Phys. Commun. **252**, 107128 (2019).
[35] C. Nielsen, Comput. Phys. Commun. **278**, 108425 (2022).
[36] P. A. Doyle and P. S. Turner, Acta Crystallogr., Sect. A **24**, 390 (1968).
[37] J. U. Andersen, Notes on channeling (2018), Lecture notes, Aarhus University, https://phys.au.dk/publikationer/lecture-notes/.
[38] A. H. Sørensen, Nucl. Instrum. Methods Phys. Res., Sect. B **119**, 2 (1996).
[39] C. F. Nielsen, R. Holtzapple, and B. King, Phys. Rev. D **106**, 013010 (2022).
[40] J. Lindhard, Mat. Fys. Medd. Dan. Vid. Selsk **34**, 1 (1965), http://gymarkiv.sdu.dk/MFM/kdvs/mfm%2030-39/mfm-34-14.pdf.
[41] T. N. Wistisen, A. Di Piazza, C. F. Nielsen, A. H. Sørensen, and U. I. Uggerhøj (CERN NA63 Collaboration), Phys. Rev. Res. **1**, 033014 (2019).
[42] A. Di Piazza, C. Müller, K. Z. Hatsagortsyan, and C. H. Keitel, Rev. Mod. Phys. **84**, 1177 (2012).
[43] J. D. Jackson, *Classical Electrodynamics* (Wiley, New York, 1975).
[44] B. King and H. Ruhl, Phys. Rev. D **88**, 013005 (2013).
[45] G. Torgrimsson, Phys. Rev. D **102**, 096008 (2020).
[46] V. Dinu and G. Torgrimsson, Phys. Rev. D **97**, 036021 (2018).
[47] B. King and A. M. Fedotov, Phys. Rev. D **98**, 016005 (2018).
[48] B. King, N. Elkina, and H. Ruhl, Phys. Rev. A **87**, 042117 (2013).
[49] D. Seipt and B. King, Phys. Rev. A **102**, 052805 (2020).